Optics & Laser Technology 192 (2025) 114088

Contents lists available at ScienceDirect

Optics and Laser Technology

journal homepage: www.elsevier.com/locate/optlastec

Full length article

Advancing optoelectronic reservoir computing: enhancing performance through ultrafast neuromorphic hardware technologies

Lília M.S. Dias [a,b,c], Ana R. Bastos [b,e], Tiago Alves [b,d], Elias Towe [c], Rute A.S. Ferreira [a], Paulo S.B. André [b,e,*]

[a] Department of Physics and CICECO—Aveiro Institute of Materials, University of Aveiro 3810-193 Aveiro, Portugal
[b] Instituto de Telecomunicações, Instituto Superior Técnico, Universidade de Lisboa 1049-001 Lisbon, Portugal
[c] Department of Electrical and Computer Engineering, Carnegie Mellon University 15213 Pittsburgh, PA, USA
[d] ISCTE - Instituto Universitário de Lisboa (ISCTE-IUL) and Instituto de Telecomunicações, Lisboa, Portugal
[e] Department of Electrical and Computer Engineering, Instituto Superior Técnico, Universidade de Lisboa 1049-001 Lisbon, Portugal

ARTICLE INFO

Keywords:
Neuromorphic engineering
Time series predictions
Signal classification
Signal reconstruction
Reservoir computing

ABSTRACT

Reservoir computing is a neuromorphic architecture based on artificial neural networks. It has gathered significant attention due to its simplicity and efficiency in processing complex sequential data for real-world tasks. We propose an advanced optoelectronic reservoir computing system that uses a single nonlinear node comprised of a Mach-Zehnder interferometer, an optical delay line, and several high-bandwidth integrated optoelectronic components. This system shows efficient performance on benchmark tasks such as signal recognition with an accuracy of 100%, nonlinear channel equalization for generating reconstructed signals with symbol error rates of 10^{-55}, and time-series predictions that reach normalized mean square errors in the order of 10^{-2}.

1. Introduction

Research in information processing hardware has long been an area of interest. It has evolved in tandem with electronic and photonic technology advances that have opened up new research frontiers in conceptual understanding. Artificial Intelligence (AI), a key driver for this evolution, has been transforming society and technology [1]. The von Neumann architecture of conventional computers, with memory and processing units separated from each other, has become woefully inefficient as data volumes and the complexity of AI models have grown [2,3]. Inspired by the human brain, with its low power consumption of only 20 Watts, neuromorphic engineering models have emerged as new approaches to computing hardware design [4]. These models have predominantly been implemented in the electronic domain [5]. However, because they have been facing challenges in speed and energy consumption, new alternative hardware implementations are being explored [3], such as the photonic computing that exploits the exceptional properties of light (e.g., diffraction, refraction, interference, and scattering) [6]. In addition to the promise of higher speeds and energy efficiency, photonic systems are expected to enable high bandwidth interconnectivity and scalability [2].

Reservoir Computing (RC) is among the most well-known neuromorphic architectures based on physical hardware that emulate artificial neural networks (ANNs). It uses nonlinear recurrent dynamics across three layers: an input layer, a core layer, and an output layer, with only the latter being digitally trained with minimal complexity [7] (Fig. 1**.a).** The simplicity in design makes processing complex signals efficient, especially signals from sequential data, where temporal relationships are captured using feedback delay loops. The RC systems have been explored across multiple domains in both electronics and photonics. Electronic reservoirs typically use a Mackey-Glass nonlinearity with analog/digital converters as delay lines [8,9]. Optoelectronic reservoirs are generally based on Mach-Zehnder interferometers (MZIs) as nonlinear elements and optical fiber delay lines [10–13]. They also use nonlinear wavelength dynamics [14] or silicon photonics with electrical nonlinearity [15]. Other schemes are all-optical reservoirs based on MZIs with optical fibers [16] or ring resonators [17].

This study advances a previous RC architecture [10] (Fig. 1**.b)** by operating at higher sample frequencies (~12 GHz), therefore with higher temporal resolution and enabling a larger number of neurons (656) in a short delay line of 3 meters. Comparing to other RC architectures [11–13,16], the one proposed here combines a high neuron

* Corresponding author.
E-mail addresses: rferreira@ua.pt (R.A.S. Ferreira), paulo.andre@lx.it.pt (P.S.B. André).

https://doi.org/10.1016/j.optlastec.2025.114088
Received 2 July 2025; Received in revised form 3 September 2025; Accepted 7 October 2025
Available online 17 October 2025

count with a short delay line. The performance was assessed through real-world benchmark tasks that include signal classification (Fig. 1.**c**), signal reconstruction (Fig. 1.**d**), and time-series prediction (Fig. 1.**e**). This work demonstrates the effectiveness of the proposed design with improved speed, scalability, and performance, which highlights the potential of neuromorphic optoelectronic RCs as efficient auxiliary accelerators within the conventional computing paradigm.

2. Principles of reservoir computing

The RC falls within the field of ANNs, where memory and computation converge to capture salient features and time correlations of sequential input information. The three fundamental layers that comprise an RC system are the (i) input, (ii) the reservoir, and the (iii) output layer (Fig. 1.**a**). In the first layer, input signals are pre-processed and injected into the reservoir. The core of the reservoir is the second layer, comprised of N virtual neurons that process the information. At the output layer, signals from the core reservoir layer are used for a regression model training and testing [7].

The state of the reservoir is conceptually a combination of different operations and weight matrices. Before injection into the reservoir, the input vector is masked by multiplying each value of it by a random matrix, M_{in}, whose elements store different weights for each of the N neurons to break the symmetry of the system [7,10]. The internal dynamics of the reservoir are based on connections with weights W_{int} that are associated with a fading memory, i.e., a signal attenuation, α, per round-trip time, τ. The state of the reservoir, $\chi(t)$, at a given instant can be approximated by Eqn. (1), where $x_{in}(t)$ is the input data, b is a vector of biases, and $f(t)$ is a nonlinear function that describes the intrinsic dynamics [10,18].

$$\chi(t) = f[M_{in}x_{in}(t) + \alpha W_{int}\chi(t-\tau) + b] \quad (1)$$

The number of neurons N is obtained as the ratio between the round-trip time (τ) of the system and the sampling period (θ) used to feed the reservoir, Eqn. (2) [18], reflecting how many points can coexist and be processed simultaneously. Therefore, a high sampling rate and/or a high round-trip time enable an increased number of virtual neurons in the reservoir, improving performance.

$$N = \frac{\tau}{\theta} \quad (2)$$

At the output layer, where the training is performed, the state of the reservoir is correlated with a target signal through multiple linear regression calculations that minimize a loss function, i.e., trains the weights W_{out} to be optimal and used to generate the final response/prediction of the reservoir [7,10].

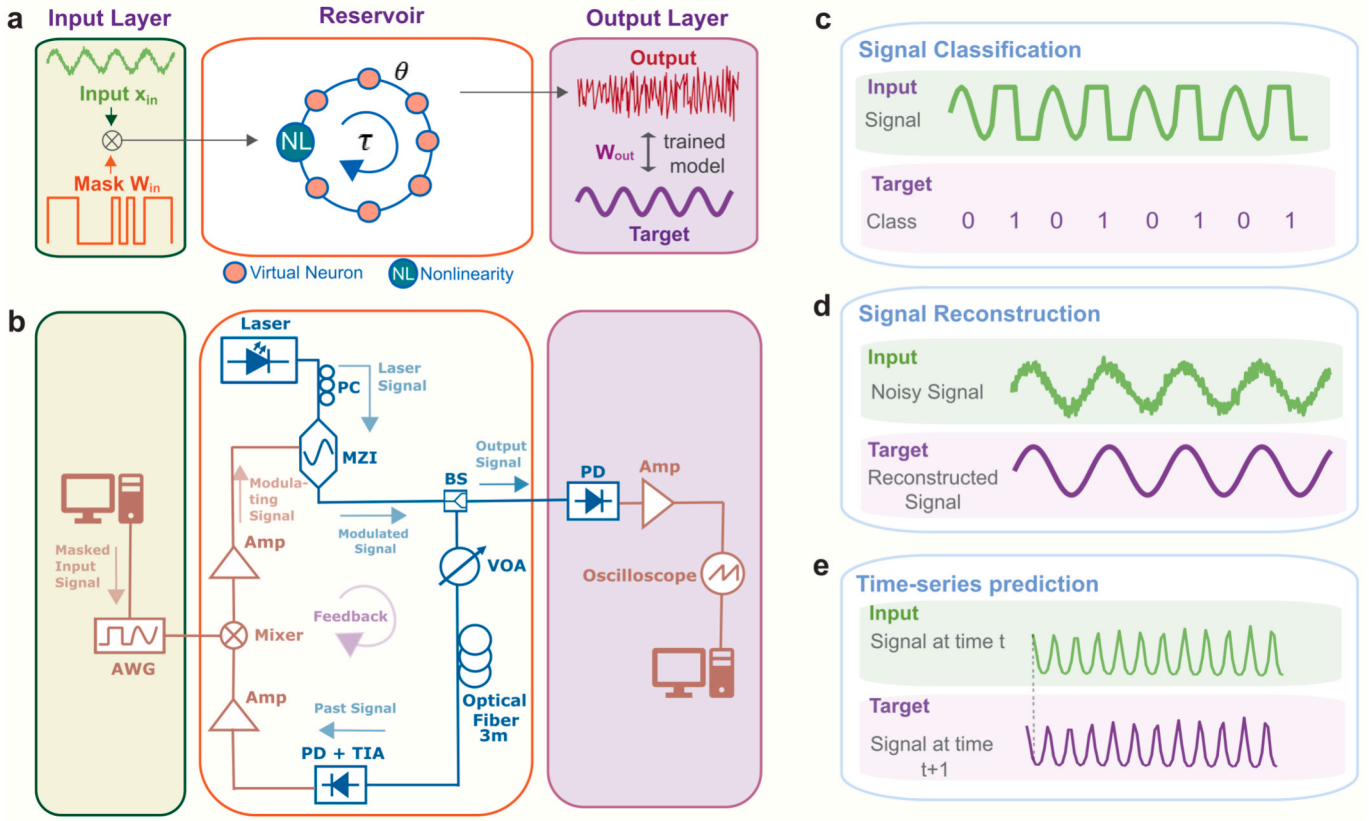

Fig. 1. Reservoir computing: (a) Schematic representation; an input signal x_{in} is multiplied (pre-processed) to provide the masked input signal, $M_{in}x_{in}$, that is fed to the reservoir; the core reservoir layer consists of a nonlinear (NL) node and a feedback fiber loop that can store N virtual neurons spaced in time by θ, and a total round-trip time of $\tau = N\theta$; the output and target signals are used to train and test a linear regression model. (b) Illustration of the experimental setup of the implemented RC system comprised of the key components: an arbitrary waveform generator (AWG), an electrical amplifier (Amp), a Mach-Zehnder Interferometer (MZI), a laser, a polarization controller (PC), a beam splitter (BS), a photodiode (PD), a variable optical attenuator (VOA), an optical fiber, a photodiode with transimpedance amplifier (PD + TIA), a mixer and an oscilloscope. The blue and orange arrows correspond to the optical and electrical signal paths, respectively. The real-world implemented tasks are the (c) signal classification, (d) signal reconstruction, and (e) time-series prediction.

3. Experimental implementation

3.1. Experimental setup

The experimental setup is depicted in Fig. 1**.b**. The input layer is where the primary signals are first generated and pre-processed before being sent to the AWG (Tektronix AWG7122B) operating at a sampling rate of 12 GS/s. At the reservoir layer, the input signal is amplified using an electrical amplifier (Model 5828A by Picosecond). The resultant signal is then used to modulate an optical signal generated in a 10 Gb/s MZI (Model T.MXHI.1-10PD-ADC-48 193337, Sumitomo Osaka Cement). The MZI modulates the optical signal from a laser emitting at 1553 nm, with a linewidth of 3 MHz (Model AP3390A, APEX Technologies), and a power of 12 dBm. The input/output characteristic transfer function of the MZI is shown in **Fig.S1**, representing the nonlinear function of the reservoir. The optical output of the MZI is split in a 50/50 ratio by a beamsplitter (Model SWFC5150P002214, Oplink). Half of the signal is sent back to the input point through a feedback loop that is comprised of a variable optical attenuator (Model FVA.600, EXFO) with attenuation fixed at 2.16 dB and a 3-meter-long single mode optical fiber (G.652). This branch of the optical signal is converted into an electrical signal with a photoreceiver (Model LabBuddy R401HG, Discovery Semiconductor). The resultant electrical signal is amplified with an electronic amplifier (Model 5828A, Picosecond Pulse Labs) and combined with the original input signal from the AWG in an electronic combining switch (mixer) with a bandwidth of 18 GHz (Model ZFRSC-183-S+, Mini Circuits). The remaining optical signal from the 50/50 beamsplitter becomes the output, and it is fed into a photodetector (Model DSC40S, Discovery Semiconductor), whose resulting electrical signal is amplified and displayed on an oscilloscope (Model DSO81204A, 12 GHz Agilent Infiniium). The amplifier gains were kept fixed at 10 dB. The feedback gain of the reservoir is − 0.7 dB. The setup settings were kept fixed during all the tasks. The system round-trip time was experimentally measured as $\tau = 54.7$ ns, yielding according to Eq. (2) to $N = 656$.

3.2. Benchmark tasks

For each task considered, input and target signals are generated for the training and testing of the reservoir. For signal classification, the input signal consists of randomly concatenated square and sinusoidal pulses, where each pulse has 12 points. The target signal is a binary array with 0/1 corresponding, respectively, to the points of the sine or square pulses. The ability of the reservoir to reconstruct signals was evaluated through the task of nonlinear channel equalization of signals with four symbols [−0.75, −0.25, 0.25, 0.75] (Section S2.1 of the Supplementary Information). The input signals were generated with signal-to-noise ratios (SNRs) of 12, 16, 20, 24, 28, and 32 dB, as well as the corresponding target signals. For each SNR value, 13,716 and 1,524 points were used for training and testing of the reservoir, respectively. In the category of time-series prediction, the reservoir was evaluated using four tasks. One task consisted of studying a Mackey-Glass system (Supplementary Information Section S2.2 [19]). The second task was based on the dynamics of a chaotic laser, whose time series behaviour was acquired using the Santa-Fe competition method [20,21]. The third task was also included in the Santa-Fe competition (heart rate record) [22–24]. The targets consisted of input signals shifted by one time step ahead of the original one. For each task, an average performance was computed using signals with 1,524 points, broken down to 1,219 points and 305 points for training and testing, respectively. The fourth task implemented was the nonlinear autoregressive moving average (NARMA) constituted from a random sequence of white noise signals. The target was a nonlinear autoregressive moving average model, which considered past and present information (Equation S4 in Supplementary Information, Section S2.3) [25]. For signal classification, nonlinear channel equalization and NARMA time series prediction, the signals with length 13,716 points result from a concatenation of nine input sequences of 1,524 points that were individually processed by the reservoir. The concatenation of signals was made to increase the size of the training sets. For nonlinear channel equalization, the correlations between the input sequences of 1,524 points were evaluated (**Fig.S2**, Supplementary Information) revealing low correlation values (∼0.1), ensuring that the reservoir's robustness was assessed across highly independent signals with the same SNR.

At the input layer, the signal is pre-processed into a high-dimensional state that can be handled by the N virtual neurons of the reservoir. The mask, W_{in}, is a $1 \times N$ randomly generated array, whose values depend on the application. We evaluated two random masks proposed in the literature [18] and selected the one providing superior performance. For signal classification and time-series prediction, random values were drawn from a normal distribution in [0, 1], while for signal reconstruction they were drawn from [−1, 1]. At the output layer, the readout training creates multiple linear regression models between the outputs to corresponding targets and the optimized regression coefficients are then applied to make predictions on new testing datasets. The linear regression was computed based on ordinary least squares objective functions.

The size of the training and testing datasets differ for each task. Post-processing of predictions is often required, as in the case of signal classification. In this case, each square/sinusoidal pulse consists of 12 points, generating 12 predictions that are integrated into a single predicted value per pulse. A threshold level for post-processing was applied: a histogram of the predictions was computed, and probability density functions (pdfs) approximately centred at the discrete levels of 0/1 were fitted. The optimal level of separation between the pdfs was calculated and used as a threshold to determine the final predictions. The performance of the reservoir is assessed by comparing the final predictions of the reservoir to the target signals in the training and testing. The performance was evaluated using accuracy for signal classification (Eq. S5), SER for signal reconstruction (Eq. S6), and NMSE for time-series prediction (Eq. S7, Supplementary Information), following typical procedures in the literature (Table S1, Supplementary Information).

4. Results and Discussion

4.1. Signal classification

The pattern recognition capability of the RC was evaluated through a signal classification task. Examples of the original and masked input signals, along with the corresponding reservoir output, are shown in Fig. 2**.a-c**, respectively. The reservoir testing predictions (Fig. 2**.d**) are post-processed through integration in blocks of 12 points that form each pulse (Fig. 2**.e**), and the corresponding histograms and fitted pdfs were computed to obtain the optimal separation level (Fig. 2**.f**). The separation level obtained was used as a threshold for determining the final predictions of 0/1, as shown in Fig. 2**.g**. The performance of the RC for this task achieved an accuracy of 100% in training (**Fig.S3**, Supplementary Information) and testing.

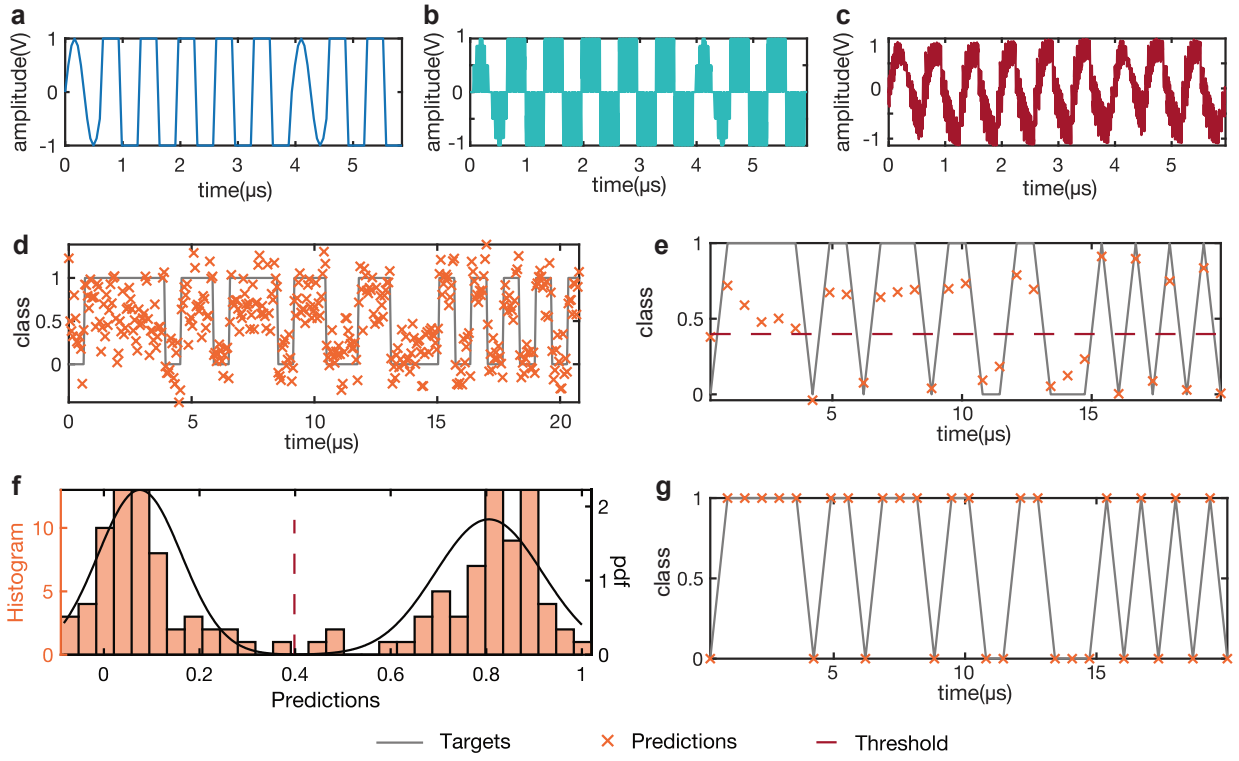

Fig. 2. Signal Classification. Segment of the a) original input, b) masked input and c) corresponding reservoir output signals used in the testing of the RC; reservoir predictions d) before and e) after post-processing by integrating in blocks of 12 points; f) histogram and fitted pdfs to the processed predictions with the optimal level of separation used as a threshold to obtain the g) final test predictions.

4.2. Signal reconstruction

The proposed reservoir was evaluated in the reconstruction of signals that went through a noisy nonlinear channel. As an illustrative example, consider the case for an input signal with SNR = 12 dB. Fig. 3.**a** shows the histogram of the input signal, with a high overlap between the Gaussian pdfs of each symbol value, yielding SER = 5.2×10^{-6}. Testing the reservoir produced a reconstructed signal, with its distribution shown in Fig. 3b. Each symbol is clearly distinguishable in the pdf, as further supported by the comparison of predictions versus the target signal in Fig. 3c, accompanied by a reduced SER (2.4×10^{-20}). The SERs for the original and reconstructed signals were obtained for different SNR values (**Fig.S4-S5**, Supplementary Information), revealing an improvement in the reconstructed signals with SER values down to 2.3×10^{-55} for SNR = 32 dB (Fig. 3.**d**), proving the usefulness of the reservoir and its potential to perform nonlinear channel equalization.

4.3. Time-series prediction

Three time-series datasets were used, namely the Mackey-Glass

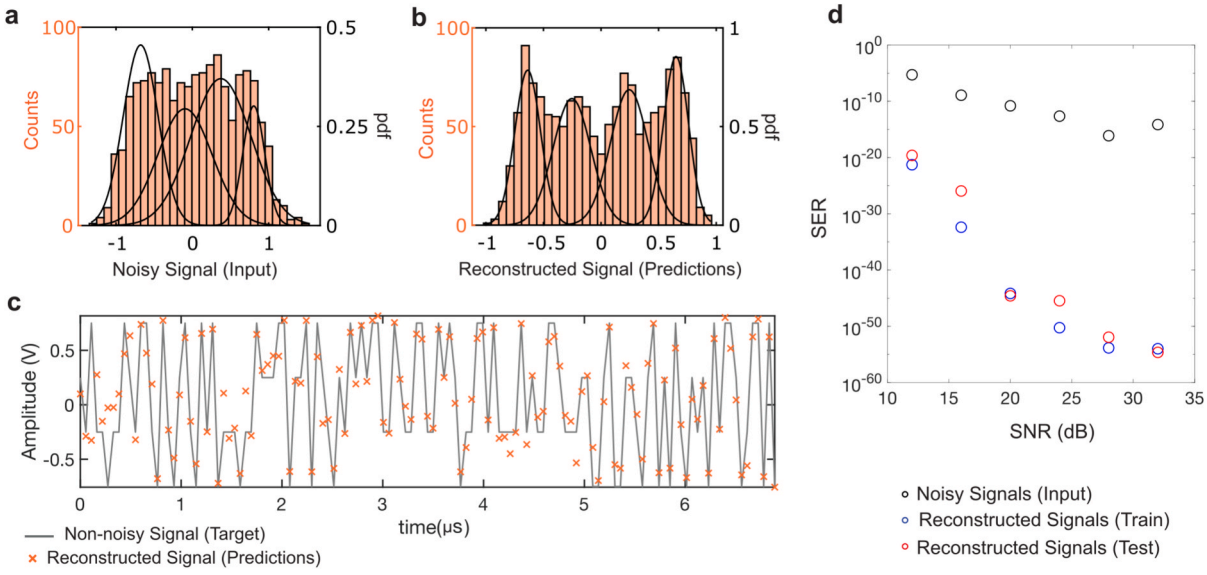

Fig. 3. Nonlinear channel equalization. Histogram and fitted probability density functions of the a) input signal with SNR of 12 dB and the b) reconstructed signal (testing predictions); c) symbol targets and testing predictions; d) SER of the input and reconstructed signals in training and testing as a function of the SNR.

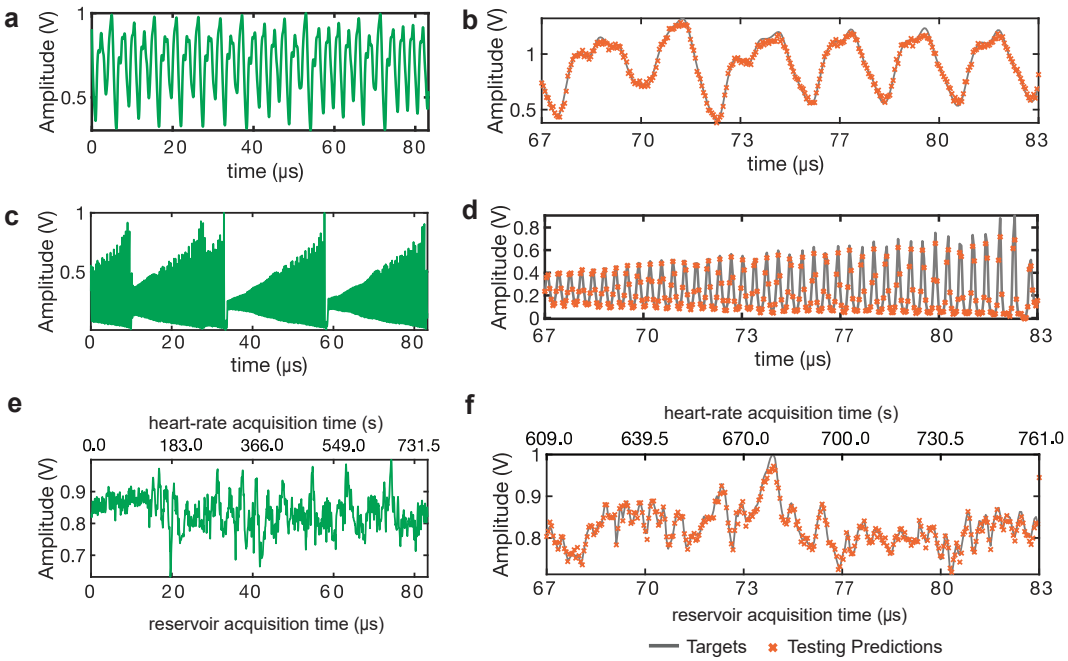

Fig. 4. Time series predictions. Illustrative examples of the time series used in a) Mackey-Glass, and Santa Fe c) chaotic laser, and e) heart rate beat; b),d),f) target signals (input signals shifted one timestep forward) versus the testing predictions from the reservoir, respectively; in e),f) the time scale is shown for the heart-rate acquisition frequency (2 Hz) and for the reservoir acquisition sampling rate (12 GHz).

system (Fig. 4a), a chaotic far-infrared laser (Fig. 4c), and a heart rate record from a suspected sleep apnea case (Fig. 4e), the latter two from the Santa Fe time-series competition [25]. In this example, the conceptualization of the target signals differs as the inputs are time-series, and the targets are time-series shifted by one time-step to the future. Fig. 4**.b,d,f** show the testing predictions for the Mackey-Glass, chaotic laser, and heart rate datasets, yielding NMSEs of 1.6×10^{-2}, 1.2×10^{-2}, and 2.4×10^{-1}, respectively (the corresponding training results are shown in **Fig.S6** in Supplementary Information). In a fourth task, we evaluated the NARMA-10 benchmark, a time-series prediction problem where the input is a random sequence and the target is generated by a nonlinear autoregressive moving average model. This task tests the reservoir's ability to capture the memory of the past 10 time-steps [25], yielding NMSE $= 4.6 \times 10^{-1}$ during the test phase (**Fig. S7**).

5. Summary

A reservoir for neuromorphic computing was constructed using high-speed optoelectronic components, enabling operation at 12 GHz and the use of a 3-meter optical fiber delay line for efficient feedback. This compact delay line allows for a more efficient and scalable system design. The computational power of the reservoir arises from a large number of virtual neurons (656) confined within the system. The system achieved 100% accuracy in signal classification and a SER on the order of 10^{-55} for nonlinear channel equalization. It also demonstrated low NMSE values in time-series prediction tasks for Mackey-Glass, Chaotic Laser, heart-rate beat, and NARMA-10 time series. The proposed reservoir achieves superior performance despite the short delay line. Operating at high sampling frequencies allows for a high neuron count, which directly enhances computational capacity. The performance demonstrates that the system is not only a versatile, multi-purpose reservoir but also particularly suited for tasks requiring high precision and efficiency. Furthermore, the work highlights the potential for developing specialized optoelectronic reservoirs optimized for specific applications, opening new pathways for high-performance neuromorphic computing systems.

CRediT authorship contribution statement

Lília M.S. Dias: Writing – original draft, Methodology, Investigation. **Ana R. Bastos:** Writing – original draft, Methodology, Investigation. **Tiago Alves:** Investigation. **Elias Towe:** Writing – original draft, Supervision. **Rute A.S. Ferreira:** Writing – original draft, Supervision. **Paulo S.B. André:** Writing – original draft, Supervision, Methodology, Investigation, Conceptualization.

Declaration of competing interest

The authors declare that they have no known competing financial interests or personal relationships that could have appeared to influence the work reported in this paper.

Acknowledgments

This work was developed within the scope of the project CICECO – Aveiro Institute of Materials, UID/50011/2025 & LA/P/0006/2020 (DOI 10.54499/LA/P/0006/2020), financed by national funds through the FCT/MCTES (PIDDAC) and Instituto de Telecomunicações, UID/50008/2025 (10.54499/UID/50008/2025), and LA/P/0109/2020 (DOI: 10.54499/LA/P/0109/2020). LMSD thanks FCT for the PhD grant UI/BD/153491/2022, (DOI:10.54499/UI/BD/153491/2022), financed by national funds through the FCT/MEC (PIDDAC), and when appropriate, cofinanced by FEDER under the PT2020 Partnership through European Regional Development Fund (ERDF) in the frame of Operational Competitiveness and Internationalization Programme (POCI). ARB acknowledges financial support by IT-Lisbon and FCT under Contract No. CEECINST/00058/2021/CP2816/CT0004 (DOI:10.54499/CEECINST/00058/2021/CP2816/CT0004).

Appendix A. Supplementary data

Supplementary data to this article can be found online at https://doi.org/10.1016/j.optlastec.2025.114088.

Data availability

Data will be made available on request.

References

[1] D. Garisto, How cutting-edge computer chips are speeding up the AI revolution, Nature 630 (8017) (2024) 544–546.
[2] C. Li, X. Zhang, J. Li, T. Fang, X. Dong, The challenges of modern computing and new opportunities for optics, PhotoniX 2 (1) (2021) 20.
[3] D. Kudithipudi, C. Schuman, C.M. Vineyard, T. Pandit, C. Merkel, R. Kubendran, J. B. Aimone, G. Orchard, C. Mayr, R. Benosman, J. Hays, C. Young, C. Bartolozzi, A. Majumdar, S.G. Cardwell, M. Payvand, S. Buckley, S. Kulkarni, H.A. Gonzalez, G. Cauwenberghs, C.S. Thakur, A. Subramoney, S. Furber, Neuromorphic computing at scale, Nature 637 (8047) (2025) 801–812.
[4] K. Roy, A. Jaiswal, P. Panda, Towards spike-based machine intelligence with neuromorphic computing, Nature 575 (7784) (2019) 607–617.
[5] D. Ivanov, A. Chezhegov, M. Kiselev, A. Grunin, D. Larionov, Neuromorphic artificial intelligence systems, Front. Neurosci. 16 (2022).
[6] R. Li, Y. Gong, H. Huang, Y. Zhou, S. Mao, Z. Wei, Z. Zhang, Photonics for Neuromorphic Computing: Fundamentals, Devices, and Opportunities, Adv. Mater. 37 (2) (2025).
[7] M. Yan, C. Huang, P. Bienstman, P. Tino, W. Lin, J. Sun, Emerging opportunities and challenges for the future of reservoir computing, Nat. Commun. 15 (1) (2024) 2056.
[8] M.C. Soriano, S. Ortin, L. Keuninckx, L. Appeltant, J. Danckaert, L. Pesquera, G. van der Sande, Delay-based Reservoir Computing: Noise Effects in a combined Analog and Digital Implementation, IEEE Trans Neural Netw Learn Syst 26 (2) (2015) 388–393.
[9] L. Appeltant, M.C. Soriano, G. Van der Sande, J. Danckaert, S. Massar, J. Dambre, B. Schrauwen, C.R. Mirasso, I. Fischer, Information processing using a single dynamical node as complex system, Nat. Commun. 2 (1) (2011) 468.
[10] Y. Paquot, F. Duport, A. Smerieri, J. Dambre, B. Schrauwen, M. Haelterman, S. Massar, Optoelectronic Reservoir Computing, Sci. Rep. 2 (1) (2012) 287.
[11] L. Larger, M.C. Soriano, D. Brunner, L. Appeltant, J.M. Gutierrez, L. Pesquera, C. R. Mirasso, I. Fischer, Photonic information processing beyond Turing: an optoelectronic implementation of reservoir computing, Opt. Express 20 (3) (2012) 3241.
[12] D. Brunner, M.C. Soriano, C.R. Mirasso, I. Fischer, Parallel photonic information processing at gigabyte per second data rates using transient states, Nat. Commun. 4 (1) (2013) 1364.
[13] X. Yuan, L. Jiang, L. Yan, S. Li, L. Zhang, A. Yi, W. Pan, B. Luo, The optoelectronic reservoir computing system based on parallel multi-time-delay feedback loops for time-series prediction and optical performance monitoring, Chaos Solitons Fractals 186 (2024) 115306.
[14] R. Martinenghi, S. Rybalko, M. Jacquot, Y.K. Chembo, L. Larger, Photonic Nonlinear Transient Computing with Multiple-Delay Wavelength Dynamics, Phys. Rev. Lett. 108 (24) (2012) 244101.
[15] K. Vandoorne, P. Mechet, T. Van Vaerenbergh, M. Fiers, G. Morthier, D. Verstraeten, B. Schrauwen, J. Dambre, P. Bienstman, Experimental demonstration of reservoir computing on a silicon photonics chip, Nat. Commun. 5 (1) (2014) 3541.
[16] F. Duport, B. Schneider, A. Smerieri, M. Haelterman, S. Massar, All-optical reservoir computing, Opt. Express 20 (20) (2012) 22783.
[17] C. Mesaritakis, V. Papataxiarhis, D. Syvridis, Micro ring resonators as building blocks for an all-optical high-speed reservoir-computing bit-pattern-recognition system, J. Opt. Soc. Am. B 30 (11) (2013) 3048.
[18] G. Van der Sande, D. Brunner, M.C. Soriano, Advances in photonic reservoir computing, Nanophotonics 6 (3) (2017) 561–576.
[19] H. Ren, Y. Li, M. Li, M. Gao, J. Lu, C.-L. Zou, C.-H. Dong, P. Yu, X. Yang, Q. Xuan, Photonic time-delayed reservoir computing based on series-coupled microring resonators with high memory capacity, Opt. Express 32 (7) (2024) 11202.
[20] A.S. Weigend, "Lorenz-like Chaos in NH3-FIR Lasers (Data Set a)," in *Time Series Prediction: forecasting the Future and Understanding the past*, Routledge, 2018.
[21] J. McNames (n.d.), "McNames Data Sets," http://web.cecs.pdx.edu/mcnames/DataSets/index.html.
[22] A. S. Weigend, "Multi-Channel Physiological Data: Description and Analysis (Data Set B)," in *Time Series Prediction: Forecasting The Future And Understanding The Past*, A. S. Weigend and N. A. Gershenfeld, eds. (Routledge, 2018), pp. 105–129.
[23] A.L. Goldberger, L.A.N. Amaral, L. Glass, J.M. Hausdorff, P.C. Ivanov, R.G. Mark, J. E. Mietus, G.B. Moody, C.-K. Peng, H.E. Stanley, PhysioBank, PhysioToolkit, and PhysioNet, Circulation 101 (23) (2000).
[24] PhysioNet, "Santa Fe Time Series Competition Data Set B," https://physionet.org/content/santa-fe/1.0.0/.
[25] C. Wringe, M. Trefzer, S. Stepney, "Reservoir computing benchmarks: a tutorial review and critique," International Journal of Parallel, Emergent and Distributed Systems 1–39 (2025).